ECCOMAS Congress 2016
VII European Congress on Computational Methods in Applied Sciences and Engineering
M. Papadrakakis, V. Papadopoulos, G. Stefanou, V. Plevris (eds.)
Crete Island, Greece, 5–10 June 2016

AN INTRODUCTION TO STOCHASTIC FINITE ELEMENT METHOD ANALYSIS OF HYPERELASTIC STRUCTURES

Marcin M. Kamiński[1], **Damian K. Sokołowski**[1],

Lodz University of Technology, Department of Structural Mechanics
Al. Politechniki 6, 90-924 Łódź, Poland
e-mail: Marcin.Kaminski@poczta.p.lodz.pl, sokolowski.dmn@gmail.com

Keywords: Stochastic Finite Element Method, hyperelasticity, rubber-like materials.

Abstract. *The main idea of this work is to demonstrate an application of the generalized iterative stochastic perturbation technique to numerical analysis of the hyperelastic materials and structures with Gaussian random parameter, where the input random variable is a magnitude of the vertical uniformly distributed load. Theoretical apparatus is connected with the general order Taylor expansion of both input and state parameters with random coefficients and analytical derivation of their first four probabilistic moments and coefficients. Our computational implementation is released with the Response Function Method having polynomial basis of the order minimizing variance and maximizing correlation of the least squares fitting to the series of numerical experiments. Computational experiment concerns the hyperelastic rubber-like prismatic beam under three-point bending discretized in the FEM system ABAQUS with the use of various 3D brick finite elements. Large deformations in the vertical symmetry plane of this structure are analyzed in the stochastic context – by determination of their expectations, coefficients of variations, skewness and kurtosis for different increments of the external load. It enables also to recover the basic probabilistic characteristics of the stress-strain curve of such a material, whose further comparison with the experiments will allow a full validation of such a probabilistic model. The entire probabilistic algorithm together with statistically optimized Weighted Least Squares Method fitting are implemented in the symbolic algebra package MAPLE. The proposed scheme of the Stochastic Finite Element Method is contrasted with the crude Monte-Carlo scheme and also with the semi-analytical calculations of the same probabilistic characteristics by direct integration of the response functions.*

1 INTRODUCTION

Modern probabilistic computational mechanics focuses on a development of the new, still more efficient theoretical and numerical methods as well as on their applications in experimentally driven models or on these research problems where the input statistics are available. Statistical nature of structural properties obviously necessary for realistic durability analysis and property prediction of materials is almost perfectly known for the area of elastic homogeneous materials but still deserves some attention in hyperelastic, visco-elastic [1], elasto-plastic, elasto-visco-plastic and especially in thermo-elasto-visco-plastic models. Although some stochastic models are known in thermal transient processes for temperature independent and dependent cases [2], a full coupling in-between elastic and thermal analysis in terms of coupled problem is still to be performed also in terms of uncertainty in temperature affecting all material and physical characteristics in terms of coupled analyses. A little bit separate problem is an identification of all material characteristics for the hyperelastic solid that needs more material constants than their elastic counterpart; the statistical point of view seems to be quite natural in this context [3], even accounting for the neural networks employed to provide such an identification [4]. Deterministic constitutive models in the area of hyperelasticity relevant to the rubber-like materials are quite well known and systematically documented. They include the Neo-Hooekan [5], Mooney-Rivlin [6], Ogden [7], Yeoh [8], Gent [9], Arruda-Boyce [10] as well as the very recent so-called extended tube model [11] resulting from molecular statistical-mechanical approach for rubber networks provided by Henrich and Kaliske. They have some Finite Element Method implementations and applications [11] that concern only an entirely deterministic case; even for a composite made of particle-reinforced rubber [12]. Probabilistic counterparts of nonlinear material models [13] are definitely less known and not systematically worked out [14] (some exceptional Monte-Carlo simulations are available but they return only quantitative results), so that such a systematic extension would be necessary. The very important aspect is that the aforementioned theories of hyperelastic behavior contain various numbers of material parameters, so that their comparisons in terms of material uncertainty will not be so straightforward as in linear elastic case; such a study needs definitely more experimental work and theoretical assumptions than before.

The main objective of this work is application of the iterative generalized stochastic 10^{th} order perturbation technique [15] implemented together with the Finite Element Method [16, 17, 18] to calculate the first four probabilistic characteristics of the ultimate vertical displacement and the corresponding Huber-Mises stress for the three-point bended hyperelastic beam. This study is undertaken to analyze the hyperelastic material with Mullins effect subjected to large deformations in a large-strain non-linear analysis with a complex contact properties and stabilization of computation. This example is also focused on numerical error determination of the FEM solution for various 3D brick finite elements and an increasing discretization density; it is also concentrated on a sensitivity analysis of the ultimate vertical displacement and the corresponding Huber-Mises stress in addition to the magnitude of an external vertical load. Probabilistic considerations included in this work are based on the Weighted Least Squares Method (WLSM) with the polynomial basis, whose order is statistically optimized and relates the displacement and stress with the uncertain external load. These optimal polynomials are then used in the iterative perturbation-based SFEM, Monte-Carlo and semi-analytical integration technique in order to determine expectations, coefficients of variation, skewness and kurtoses of the vertical deflections and the corresponding stresses in the function of the input coefficient of variation. Such a study is carried out to determine accuracy of the iterative perturbation method in analyses of hyperelastic materials and to check the probabilistic properties of the output variables, i.e. the ultimate vertical deflec-

tions and the corresponding Huber-Mises stresses. Such iterative generalized Stochastic Perturbation (SPT) method is applied here since it yields more accurate results than the classical SPT, including the negative and mixed moment terms that are absent in the linearized version. The input random parameter is chosen here as an external load in a form of the uniform pressure, whose Probability Density Function (PDF) is Gaussian. Such a parameter has been chosen here, since it is one of the most unpredictable variables included in the model. It usually cannot be exactly calculated in real structures and it varies non-monotonously with large time variations and its underestimation may certainly cause an overall failure. This is the case of civil engineering structures, machinery, vehicles or aircrafts. This work serves as a preliminary study for further expansion towards experimentally-calibrated hyperelastic material model probabilistic analysis based on a crack initiation or rubber softening.

2 HYPERELASTIC MATERIAL MODEL

Let us consider the total strain energy U in some material, which is defined as

$$U = U_{dev}\left(\lambda_i\right) + U_{vol}\left(J^{el}\right), \tag{1}$$

where U_{dev} stands for the deviatioric part of the strain energy and U_{vol} for the volumetric part of this energy. The Yeoh material definition defines these variables in a following way

$$U_{dev}\left(\lambda_i\right) = C_{10}(\overline{I}_1 - 3) + C_{20}\left(\overline{I}_1 + 3\right)^2 + C_{30}\left(\overline{I}_1 - 3\right)^3 \tag{2}$$

and

$$U_{vol}\left(J^{el}\right) = \frac{1}{D_1}\left(J^{el} - 1\right)^2 + \frac{1}{D_2}\left(J^{el} - 1\right)^4 + \frac{1}{D_3}\left(J^{el} - 1\right)^6, \tag{3}$$

in which C_{io} and D_i are temperature-dependent material parameters, $\overline{I}_1$ stand for the first deviatioric strain invariant defined as $\overline{I}_1 = \overline{\lambda}_1^2 + \overline{\lambda}_2^2 + \overline{\lambda}_3^2$ and where the stretches $\overline{\lambda}_i$ are defined as $\overline{\lambda}_i = J^{-\frac{1}{3}}\lambda_i$. J stands here for the total volume ratio and λ_i are the principal stretches. The initial shear modulus and bulk modulus are given as $\mu_0 = 2C_{10}$, $K_0 = 2/D_1$. When a thermal dependence is taken into consideration, the elastic volume ratio J^{el} relates the total volume ratio J and the thermal volume ratio J^{th} in a following manner $J^{el} = J/J^{th}$, where $J^{th} = \left(1 + \varepsilon^{th}\right)^3$. ε^{th} stands for the linear thermal expansion strain obtained from the temperature and the isotropic thermal expansion coefficient; it is not considered here.

The augmented Mullins effect strain energy density function applied in this study is following

$$U = \eta U_{dev}\left(\lambda_i\right) + \Phi\left(\eta\right) + U_{vol}\left(J^{el}\right), \tag{4}$$

where the damage variable η is defined as

$$\eta = 1 - \frac{1}{r} erf\left(\frac{U_{dev}^m - U_{dev}}{m + \beta U_{dev}^m}\right) \tag{5}$$

and the damage function is adopted here as

$$\Phi(\eta) = \int_1^n f\left(\eta, U_{dev}^n\right) d\eta + (1-\eta) U_{dev}^m, \tag{6}$$

which on the primary path $\eta = 1$ and satisfying the requirement $\Phi(1) = 0$ can be expressed as

$$\Phi'(\eta) = \left(m + \beta U_{dev}^m\right) erf^{-1}\left(r(1-\eta)\right) - U_{dev}^m. \tag{7}$$

The variables r, β and m all denote the input material constants, the first two of which are dimensionless and the latter has dimensions of energy. The error function erf used in this definition is defined as $erf(x) = \frac{2}{\sqrt{\pi}} \int_o^x \exp\left(-w^2\right) dw$ and the function $f\left(\eta, U_{dev}^n\right)$ can be further expressed as $f\left(\eta, U_{dev}^m\right) = \Phi'(\eta) + U_{dev}^m = U_{dev}^m - U_{dev} = -\Phi'(1) - U_{dev}$. Fundamental properties of this damage function are that (a) when $U_{dev}^m = U_{dev}$, then it corresponds to a point on the primary curve and $\eta = 1.0$ (b) η attains its minimum value η_m upon complete removal of deformation, i.e. when $U_{dev} = 0$ and (c) in all other cases η varies monotonously from η_m to 1.0.

3 COMPUTATIONAL EXPERIMENTS AND DISCUSSION

3.1 Computational model

A computational model applied in this study consists of three elements, the 10 m long hyperelastic beam with section of 1.5 m x 1 m, the support cylinders with diameter of 1.2 m and a 0.3 m deep loading plate having section of 1 m x 1 m (Fig. 1). The beam is supported on the two cylinders placed on each side of the beam and loaded with various magnitude of pressure of $p = 1\ Pa$ mean value, which is applied on the upper surface of the centrally placed plate. The static scheme of three-point bending is applied here firstly because it is a usual scheme used in laboratory tests, secondly since such loading is common in various applications of cyclically loaded parts and finally as it creates regions dominated by bending and shear. Both, an upper loading plate and the cylinders are deformable and much stiffer than the beam with elastic parameters set as Young modulus $E = 10\,GPa$ and Poisson ratio $\nu = 0.3$. The hyperelastic beam has a complex material definition of the Yeoh model with the following parameters: $C_{10} = 1.326$, $C_{20} = -0.326$, $C_{30} = 0.1319$, $D_1 = 0.000725$, $D_2 = 0$, $D_3 = 0$, whose Mullins effect has the following parameters: $r = 1.1$, $m = 100$, $\beta = 0.1$. This ensures a hyperelastic behavior and cyclic softening of the beam. A connection between the elements is assured by a hard contact in the normal direction enforced by the penalty method and a penalty-driven tangential contact behavior with a friction coefficient of $\mu = 0.99$ for the cylinders- and of $\mu = 0.8$ for the plate-beam boundary; the slippage of the beam from the cylinders is prevented by tying its outer edges to the cylinder surface. A possibility of separation of the model elements after an initial and repeated contact is allowed here (surfaces are not tied after the contact). In order to keep the mechanical boundary conditions for a three-point loading, bases of the cylinders are fully restrained (no displacement or rotation allowed) and the loading plate has only the vertical displacement degree of freedom (dof) active; it further supports a sym-

metry of the loading. Additionally, the beam is divided into 8 cells to shorten the surface length of both contacts, which speeds up numerical analysis.

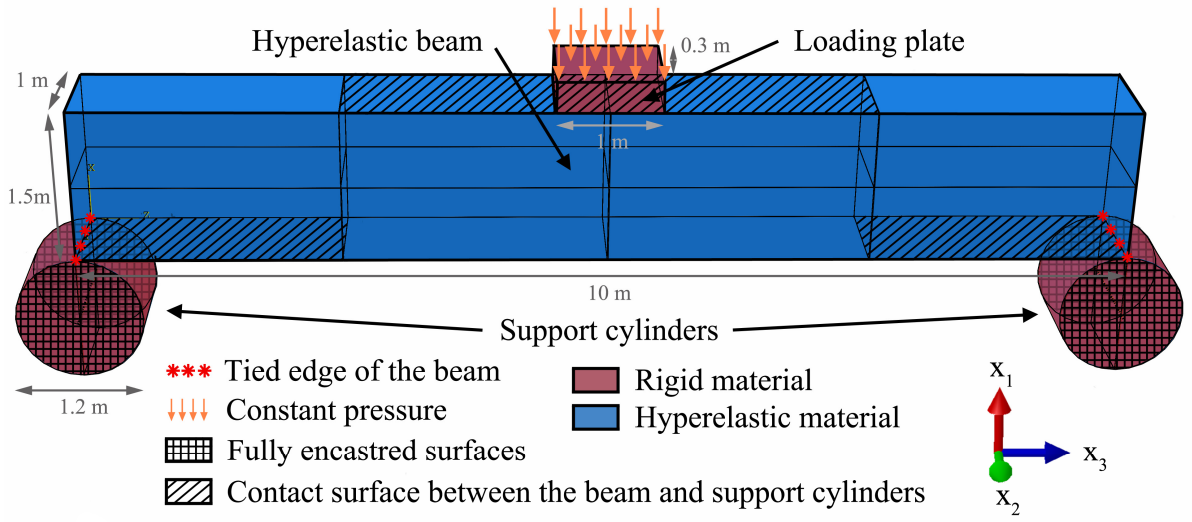

Figure 1: FEM model of the beam.

Computational model and numerical experiments are provided both in the FEM system ABAQUS with a series of beam loadings for the ultimate vertical displacement and the corresponding Huber-Mises stress of the beam. The elements are meshed with 104 397 reduced (stress) integration linear brick finite elements (C3D8R) giving a total of 418 602 independent variables (Fig. 2); the entire beam element additionally has a hybrid definition of elements of type C3D8HR, which deal with a full (or nearly full) incompressibility of this FEM domain. The type and amount of elements is selected to obtain the best possible quality of results for an acceptable computational effort via the error analysis of computational simulations presented in Fig. 4 and, separately, by a sensitivity analysis of the resulting displacements and the corresponding stress available in Fig. 5. Numerical computations include a material and contact non-linearity and are based on the non-linear theory of large strains. Completion of each simulation requires partitioning to 40-150 steps, each calculated on the basis of the result of the previous one (usually consisting of 2-16 iterations); this is a main reason for the lower amount of the Finite Elements (FEs) than in the single-step linear-elastic computations. Results of these analyses (in a form of the stress mapped on a deformed shape of the beam) show large symmetric deformations of a thick beam with also symmetric stress map – a typical work range of usual hyperelastic (rubber) materials. Predictably, the stress pattern is symmetric and the highest near the bottom of the beam; there also exist particular stress concentrations nearby the cylindrical supports and on each side of the loading plate. The stress concentrations on the support edges of the beam are disregarded in this study since they are rather enforced by the tied internal conditions and would differ for the exact type of the slippage-preventing support applied in the experiments.

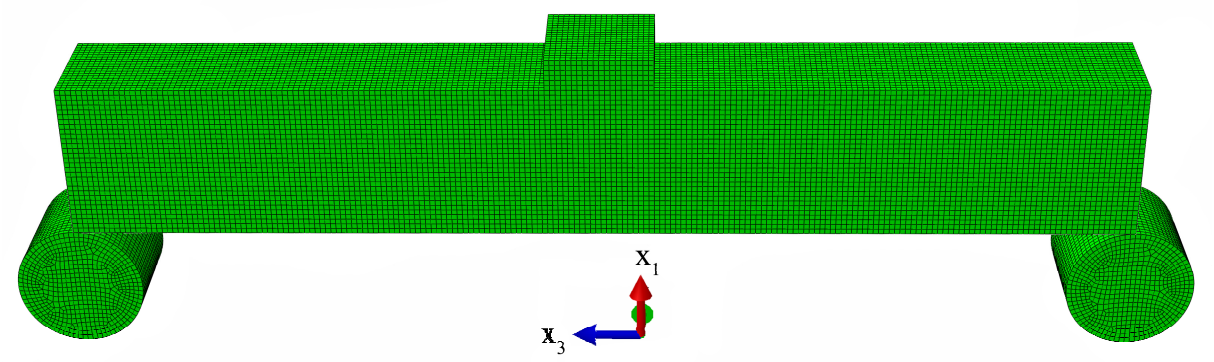

Figure 2: The finest mesh of the beam.

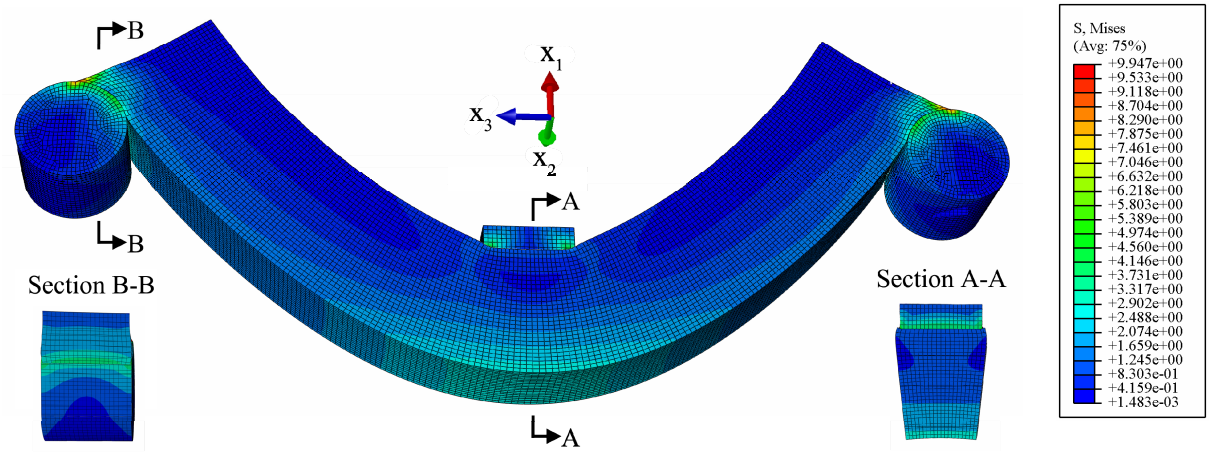

Figure 3: Map of the reduced stress plotted on deformed configuration of the beam under bending.

3.2 Computational error and sensitivity analysis

Within the error study, three types of FEs are used, i.e. the reduced integration linear brick C3D8R, the incompatible modes linear brick C3D8I and the reduced integration quadratic brick C3D20R; due to incompressibility of the material, the beam is discretized here always with the hybrid finite elements (C3D8RH, C3D8IH, C3D20RH). These particular types of elements are chosen after their best performance range, which for the linear reduced elements is large distortion in bending, for the incompatible modes – bending and for the second-order (quadratic) elements with reduced integrations - nonlinearity; all the above phenomena take place in this analysis and therefore such an error and performance study seems to be profitable here. An error graph presented in Fig. 4 firstly shows the very good convergence of results and a small error $E_r(n)$ for all the discretization densities applied, which never crosses 3% and is as small as 0.15% for the higher amount n of the FEs. The smoothness of convergence is not so evident, as in the linear analyses [20], but an overall reduction of the error together with an increase in the FEs amount is still clear. When an influence of material and contact non-linearities as well as occurrence of large strain theory is taken into consideration, this result is more than satisfactory. A secondary observable is, that in this particular case the computations of quadratic elements have a very low convergence and, additionally, that not all of the computations lead to the final result – some particular distributions of the elements are stuck in various points of the analysis. Basing on this (C3D8I brings no additional variation), the standard C3D8R elements are chosen for the further analysis. Please note, that the computational effort for the quadratic FEs is much higher than for the linear ones of the identical

amount and, therefore, Fig. 4 cannot serve for the final evaluation of time-performance of these methods.

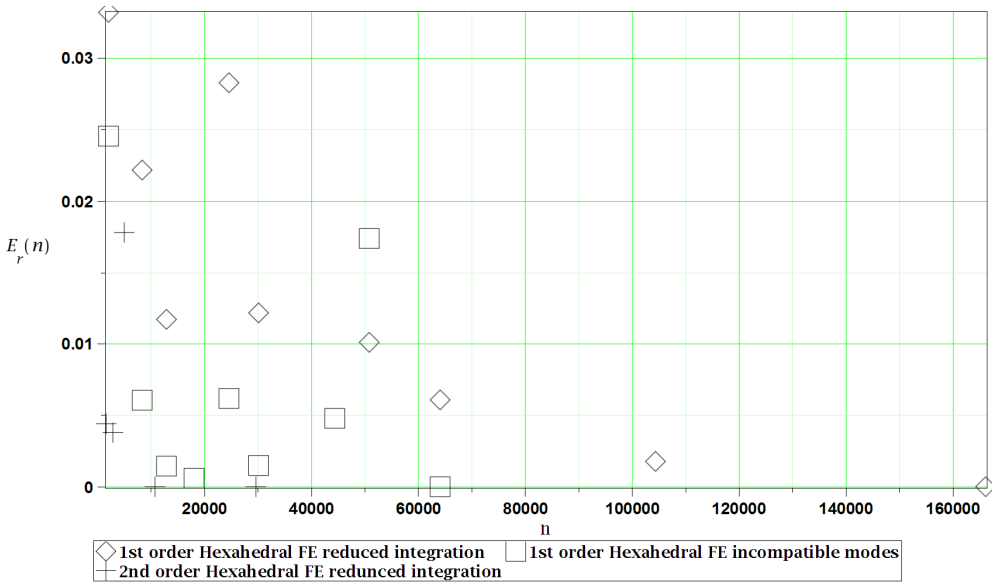

Figure 4: Computational error of the Finite Element Method results.

Sensitivity coefficients $S(p)$ of both ultimate vertical deformations and the corresponding stresses are computed by 11 separate simulations in 20% neighborhood of the mean external load, which ranges from 0.9 Pa till 1.1 Pa, via a direct algebraic differentiation based on the additional response functions (Fig. 5). These sensitivities are quite naturally all positive, since the increase of the external load should also increase both the ultimate vertical displacement and also its corresponding reduced stress. The Huber-Mises stress is much more sensitive to the fluctuations in an external load but has smaller curvature than the sensitivity of displacement in this particular load region.

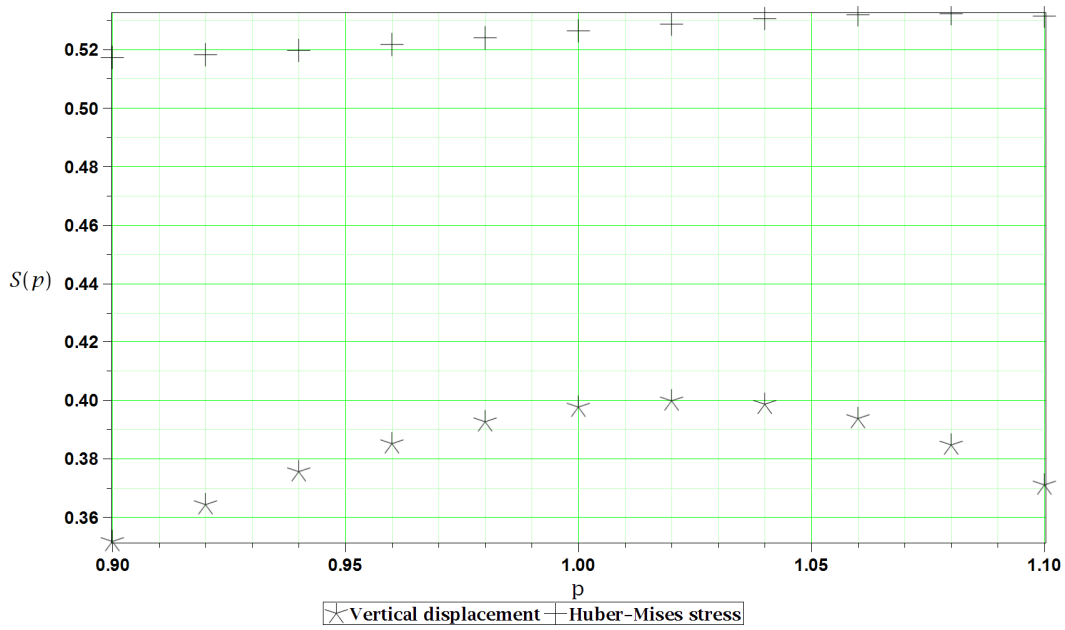

Figure 5: Sensitivity coefficients for the ultimate deformation and the corresponding von Mises stress.

3.3 Probabilistic analysis

The probabilistic computations are all carried out in the symbolic system MAPLE and are focused firstly on a determination of the optimum order of the response function of the WLSM (Tab. 1), which is then used in the main computation of the probabilistic characteristics based on the ultimate displacements and the corresponding Huber-Mises stresses. The procedure of calculation of these characteristics consists of (a) integration of the response function together with the Gaussian PDF in a semi-analytical method, (b) its insertion into the 2^{nd}, 4^{th} and 6^{th} (only for the stresses) order Taylor expansions in stochastic perturbation-based approach and (c) its sampling in a discrete Monte-Carlo analysis (with 500 000 random trials) for an increasing value of the input coefficient of variation $\alpha(p)$. The characteristics calculated in this manner include the expectation (Fig. 6), the coefficient of variation (Fig. 7), the skewness (Fig. 8) and the kurtosis (Fig. 9). The Least Squares Method is used here in its weighted form and non-linear version with a weighting scheme similar to the Dirac function – [1,1,1,1,1,10,1,1,1,1,1] – making the influence of the mean value equivalently important as the remaining test results. Maximization of the optimal polynomial order is done via simultaneous maximization of the correlation and minimization of the variance of the WLSM and the RMS error. The total number of WLSM increments equals 20 in this study and the chosen polynomial order is 4^{th} for the displacement and 5^{th} for the stress. The resulting parameters used in the optimization process are well illustrated in Tab. 1 and correlate the subsequent results with the polynomial order; all the beneath given probabilistic results (Figs 6-9) consecutively show the characteristics of the ultimate vertical displacements on the left and of the corresponding reduced (Huber-Mises) stresses on the right side. The input uncertain parameter – an external load p – varies in 20% neighborhood of the mean value of 1 Pa with 11 discrete values of $p \in [0.90,\ 0.92,\ \ldots\ ,1.00,\ \ldots\ ,1.10]$.

Variable		Vertical deformation			Huber-Mises stress		
Parameter		Correlation	Variance	RMS error	Correlation	Variance	RMS error
Polynomial order	10	0.986783	6.54E+04	3.87E+10	-0.988917	5.94E+04	2.73E+10
	9	0.99122	2.59E+03	5.39E+07	-0.985964	2.76E+02	3.88E+06
	8	-0.99389	6.80E+01	1.27E+04	-0.999826	1.78E+01	8.21E+03
	7	-0.964519	3.55E-01	2.04E+00	0.999923	1.21E-02	5.70E-03
	6	0.999816	1.11E-02	5.26E-04	0.999951	2.66E-03	3.64E-05
	5	0.999807	1.68E-03	1.02E-05	**0.999952**	**1.04E-03**	**1.34E-06**
	4	**0.999468**	**2.70E-03**	**7.94E-06**	0.999891	1.25E-03	1.70E-06
	3	0.999405	2.85E-03	8.94E-06	0.999884	1.30E-03	1.84E-06
	2	0.99539	8.00E-03	7.04E-05	0.998737	4.29E-03	2.03E-05
	1	0.999449	1.29E-01	1.83E-02	0.99989	7.63E-02	6.38E-03

Table 1: Weighted Least Squares Method optimization results for a Dirac type of weights.

The expectations of the output variables both are a little decreasing in a concave manner together with an increase of the uncertainty. Additionally, they both have a horizontal asymptote approached at the zero uncertainty, for which they obviously must return the exact results obtained in the computational FEM experiments. These output functions are continuous, smooth and with no local inflections or discontinuities. The 2^{nd} order (based on the first two Taylor expansions) perturbation-based approach returns here a little divergent results and is

valid only for $\alpha(p) \in [0.00,\ 0.05]$, but as long as the higher order is applied, all the three separate methods yield exactly the same output.

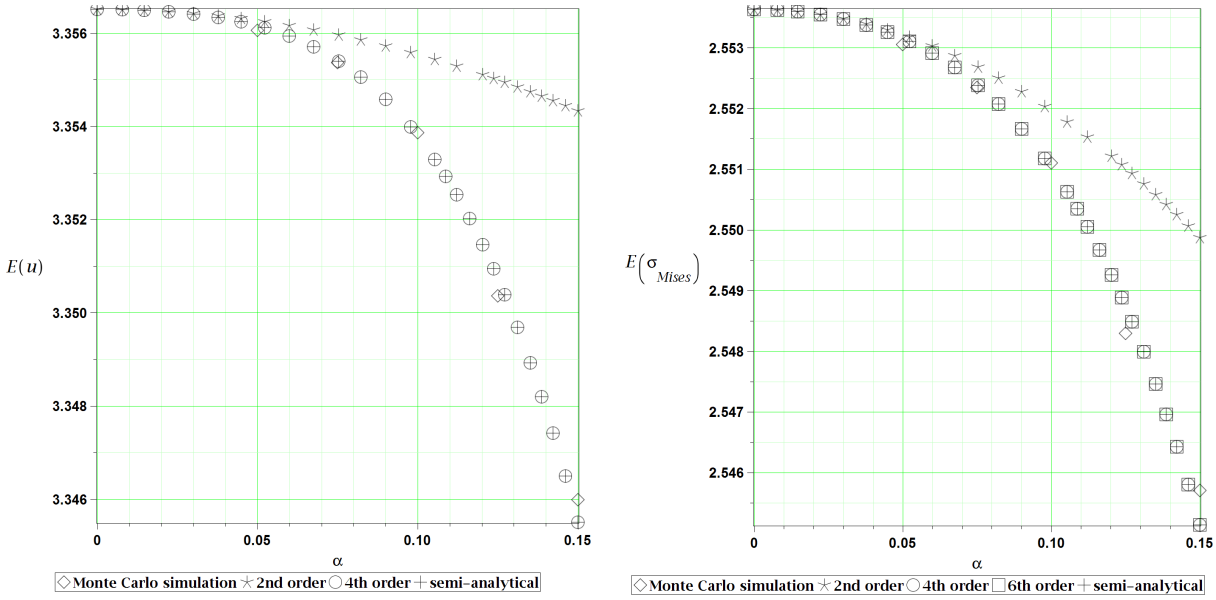

Figure 6: Expected values of
a) the ultimate deflection and b) the corresponding Huber-Mises stress
of the beam subjected to three-point bending with respect to the uncertainty in the external load.

The resulting coefficients of variation (Fig. 7) of both output variables are always increasing in the concave manner while staying lower than the input uncertainty. The differences come (a) in the curvature, which is much higher for the displacement than for the stress, (b) in the magnitude, a little smaller for the displacements, and (c) in the agreement of the probabilistic methods, being perfect for the case of the stress and not so ideal for the displacement based coefficient of variation. Predictably, the 4th order stochastic perturbation is much better correlating with the other results - up to $\alpha(p) = 0.12$, while the 2nd order – only to $\alpha(p) = 0.07$; the 6th order, available only for the stress-based characteristics, is precise for all the considered uncertainty range.

The higher order probabilistic characteristics (Figs 8-9) are generally less convergent than the previous ones. In this case not only the perturbation-based approach yields different results, but also correlation of the Monte-Carlo and semi-analytical outputs is not perfect, especially for the kurtosis based on the reduced stress. The 4th order perturbation-based approach quite early diverges – at $\alpha(p) \in [0.03,\ 0.06]$, the 6th order is much better here – it diverges only at $\alpha(p) \simeq 0.13$. Nevertheless, these higher characteristics are all smooth and without discontinuities. The 2nd order analysis disallows consideration of these higher order characteristics, since it simply vanishes. The Skewness is all negative with a rather concave manner and a small magnitude comparable for the both output characteristics. This means that both PDFs are increasingly leaning to the right side with an increase in uncertainty. Kurtoses are either only negative with an exponential manner (based on the displacement) or positive with a concave-convex curvature and an apparent inflection point at $\alpha(p) = 0.085$ (based on the stress). Since both, the kurtosis and skewness are quite close to zero, distributions of both output parameters have PDFs close, but still diverging from the normal (Gaussian) distribution for the entire uncertainty range considered here.

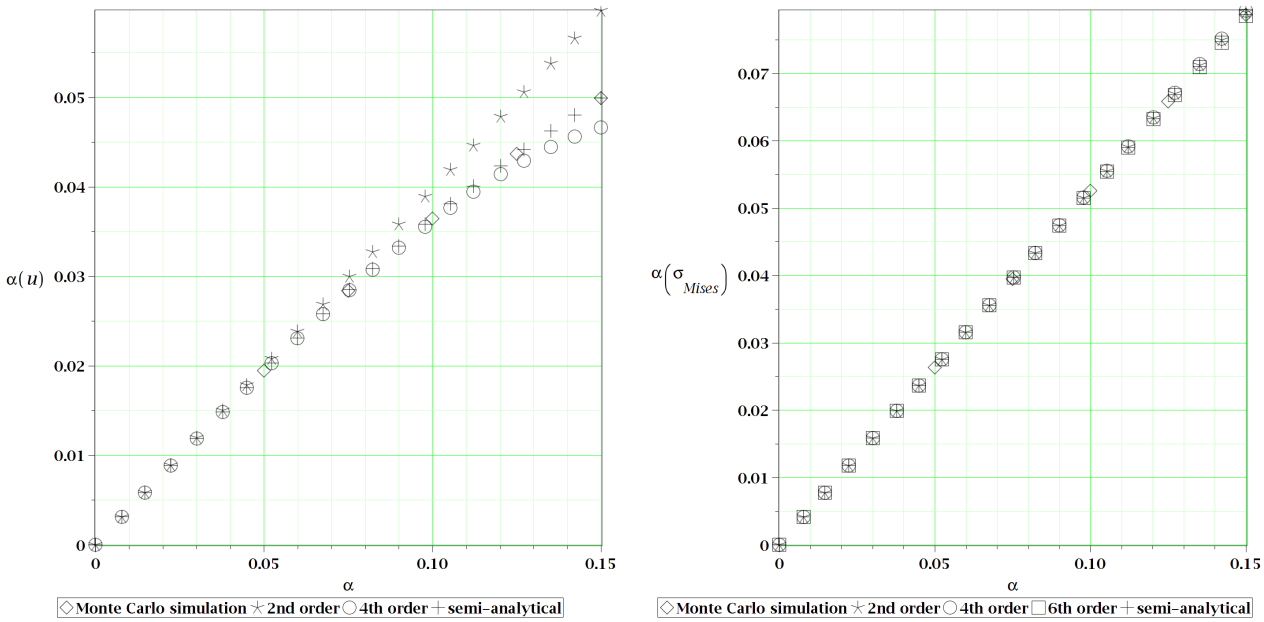

Figure 7: Coefficients of variation of
a) the ultimate deflection and b) the corresponding Huber-Mises stress
of the beam subjected to three-point bending with respect to the uncertainty in the external load.

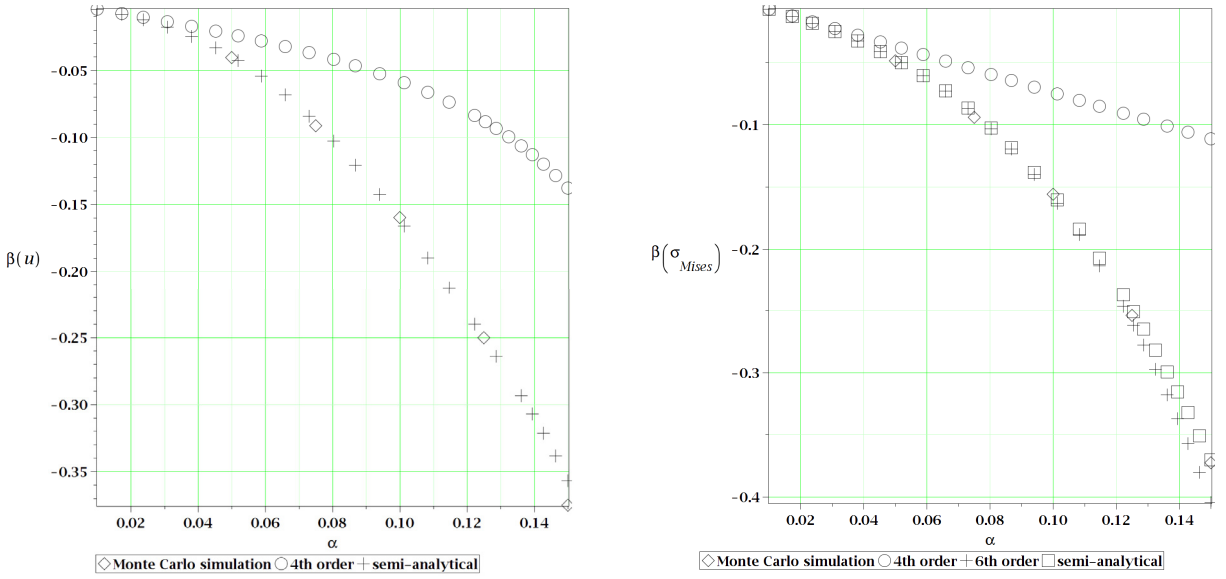

Figure 8: Skewness of
a) the ultimate deflection and b) the corresponding Huber-Mises stress
of the beam subjected to three-point bending with respect to the uncertainty in the external load.

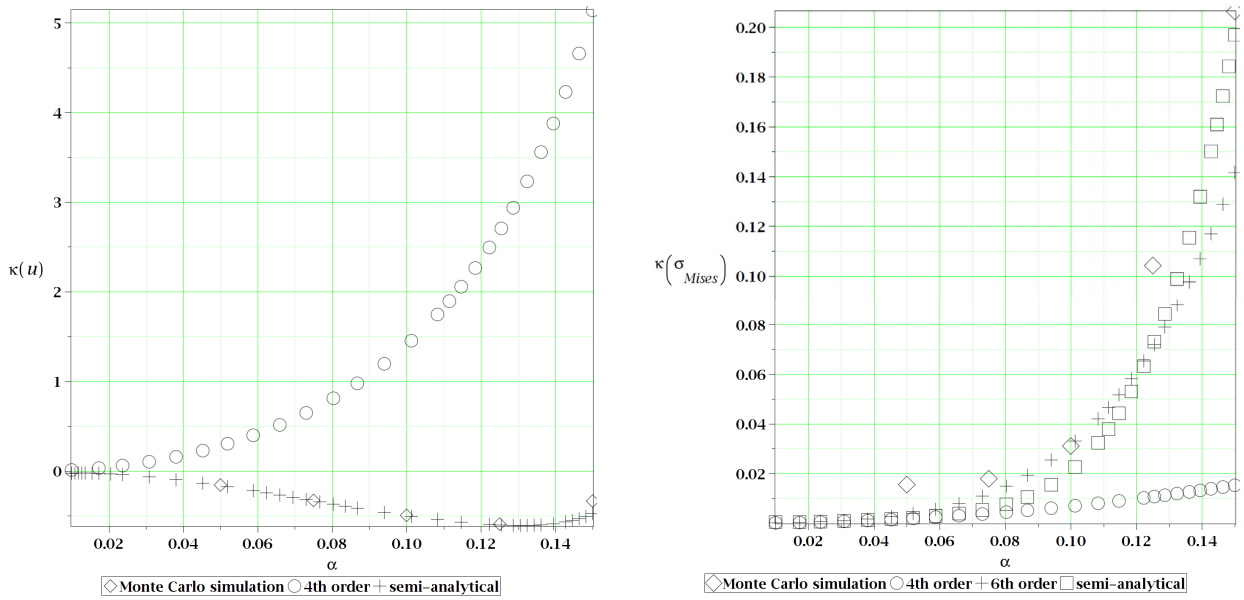

Figure 9: Kurtoses of
a) the ultimate deflection and b) the corresponding Huber-Mises stress
of the beam subjected to three-point bending with respect to the uncertainty in the external load.

4 CONCLUSIONS

This study reports calculation of the first four probabilistic characteristics of the ultimate displacements and the corresponding Huber-Mises stresses based on an input uncertain variable of the external load. The output variables are computed for the three-point bended hyperelastic beam with a Yeoh definition of material, additionally augmented by the Mullins effect. An analysis not only uses a novel iterative stochastic perturbation technique, but also connects it with a hyperelastic material in a large-strain non-linear numerical simulation. The nonlinearities come from the material, contact and constitutive relation. A further extension of this study may include (a) correlation of the material characteristics with experimental results, (b) incorporation of the fracture model in the hyperelastic material definition and (c) sequential or full coupling of this study with temperature analysis; such coupling is important here because the deformation process of elastomers is exothermic and their mechanical properties depend on temperature already in the typical environmental conditions.

Numerical analysis clearly shows that the computational error is quite small for the entire range of the FEs amount and that the preferable brick element type is C3D8R, which has a relatively high precision and provides the highest convergence for a moderate computational effort. The minimum amount of elements used in such study should generally exceed 60 000 elements, since the complex support and material definitions are susceptible to the discretization density. The resulting displacements range here from 3.22 m to 3.48 m and the Huber-Mises stresses - 2.42 Pa to 2.69 Pa for the external load in form of pressure of 0.9 Pa to 1.1 Pa. Both, the stress and the strain obtained here is much below the rupture limit for elastomers, but it certainly belongs to large deformations. Sensitivities of the displacement and Huber-Mises stress to the change in an external load are all positive and much higher for the reduced stress. Probabilistic considerations show a relatively good correspondence in-between different techniques and, predictably, an increasing correlation of the stochastic perturbation-based technique together with an increase of the length of the proposed Taylor expansion. The 6th order expansion is already almost perfectly agreeing with the remaining methods with an ex-

ception of the kurtoses higher than $\kappa(p) \simeq 0.12,$ where it slightly diverges. It should be, however, noted that this order of expansion is available only for the stresses, whose optimal response polynomial has a higher order than the one for the displacements. The probabilistic distributions of the state variables may generally be considered here as close to Gaussian, since both the Kurtosis and Skewness are quite close to zero. Nevertheless, such an assumption should rather be exceptional.

REFERENCES

[1] R. Christensen, *Theory of Viscoelasticity*. Dover Publ., Dover, 2010.

[2] T. Hien, M. Kleiber, On solving nonlinear transient heat transfer problems with random parameters, *Computer Methods in Applied Mechanics and Engineering*, **151**, 287-299, 1998.

[3] T. Harth, S. Schwan, J. Lehn, F. Kollmann, Identification of material parameters for inelastic constitutive models: statistical analysis and design of experiments. *International Journal of Plasticity*, **20**, 1403-1440, 2004.

[4] Y. Shen, K. Chandrashekhara, W.F. Breig, L.R. Oliver, Neural network based constitutive model for rubber material. *Rubber Chemistry and Technology*, **77**, 257-277, 2004.

[5] R.W. Ogden, *Non-linear Elastic Deformations*. Dover Publ., Dover, 1984.

[6] M. Mooney, A theory of large elastic deformation. *Journal of Applied Physics*, **11(9)**, 582-592, 1940.

[7] R. Ogden, D. Roxburgh, A pseudo-elastic model for the Mullins effect in filled rubber. *Proceedings of the Royal Society of London A*, **455**, 2861-2877, 1999.

[8] O. Yeoh, Some forms of the strain energy function for rubber. *Rubber Chemistry and Technology*, **66(5),** 754-771, 1993.

[9] A. Gent, A new constitutive relation for rubber. *Rubber Chemistry and Technology*, **69**, 59-61, 1996.

[10] E. Arruda, M. Boyce, A three-dimensional model for the large stretch behavior of rubber elastic materials. *Journal of the Mechanics and Physics of Solids*, **41(2)**, 389–412, 1993.

[11] M. Kaliske, G. Heinrich, An extended tube-model for rubber elasticity: statistical-mechanical theory and finite element implementation. *Rubber Chemistry and Technology*, **72**, 602-632, 2010.

[12] A. Dorfmann, R. Ogden, A constitutive model for the Mullins effect with permanent set in particlereinforced rubber. *International Journal of Solids and Structures*, **41**, 1855-1878, 2004.

[13] C. Truesdell, W. Noll, *The Non-Linear Field Theories of Mechanics. 3rd Edition*, Springer Verlag, Berlin-Heidelberg, 2004.

[14] M. Guedri, A. Lima, N. Bouhaddi, D. Rade, Robust design of viscoelastic structures based on stochastic finite element models. *Mechanical Systems and Signal Processing*, **24(1)**, 59-77, 2010.

[15] M. Kamiński *The Stochastic Perturbation Method for Computational Mechanics*, Chichester: Wiley; 2013.

[16] J.T. Oden, J.N. Reddy, *A Mathematical Theory of Finite Elements*. New York: Wiley-Intertscience; 1976.

[17] M. Kamiński, On the dual iterative stochastic perturbation-based finite element method in solid mechanics with Gaussian uncertainties. *International Journal of Numerical Methods in Engineering*, **104**, 1038-60, 2015.

[18] M. Kamiński, D. Sokołowski, Dual probabilistic homogenization of the rubber-based composite with random carbon black particle reinforcement. *Composite Structures*, **140**, 783-797, 2016.